Sioulas *et al. Water Emerg. Contam. Nanoplastics* **2025**, *4*, 5
DOI: 10.20517/wecn.2024.73

Water Emerging Contaminants & Nanoplastics

Research Article

Open Access

Photocatalytic degradation of the antidepressant drug Paroxetine using TiO_2 P-25 under lab and pilot scales in aqueous substrates

Sotirios Sioulas, Ilaeira Rapti, Christina Kosma, Ioannis Konstantinou, Triantafyllos Albanis

Department of Chemistry, University of Ioannina, Ioannina 45110, Greece.

Correspondence to: Prof. Ioannis Konstantinou, Prof. Triantafyllos Albanis, Department of Chemistry, University of Ioannina, Ioannina 45110, Greece. E-mail: iokonst@uoi.gr; talbanis@uoi.gr

How to cite this article: Sioulas, S.; Rapti, I.; Kosma, C.; Konstantinou, I.; Albanis, T. Photocatalytic degradation of the antidepressant drug Paroxetine using TiO_2 P-25 under lab and pilot scales in aqueous substrates. *Water Emerg. Contam. Nanoplastics* **2025**, *4*, 5. https://dx.doi.org/10.20517/wecn.2024.73

Received: 1 Dec 2024 **First Decision:** 17 Jan 2025 **Revised:** 13 Feb 2025 **Accepted:** 20 Feb 2025 **Published:** 26 Feb 2025

Academic Editors: Changseok Han, Joana C Prata **Copy Editor:** Pei-Yun Wang **Production Editor:** Pei-Yun Wang

Abstract

Pharmaceuticals in water bodies are a significant threat to aquatic life and human health, often persisting due to incomplete degradation in conventional wastewater treatment plants (WWTPs). Heterogeneous photocatalysis is a promising method for efficiently treating wastewater (WW). TiO_2 P-25, a well-known photocatalyst, has been widely used to remove persistent organic pollutants (POPs) from aquatic media, primarily on a laboratory scale. In this study, the photocatalytic removal of Paroxetine (PXT), an antidepressant drug, is investigated at the lab scale and pilot scale using a compound parabolic collector (CPC) reactor (85 L) working in batch recirculating mode and secondary treated hospital wastewater (HWW) as the substrate using different catalyst concentrations (200, 300, and 500 mg/L). The lab experiments achieved the fastest PXT degradation with 500 mg/L, while the pilot tests found 200 mg/L to be optimal. Thirteen transformation products (TPs) were identified using liquid chromatography-high-resolution mass spectrometry (LC-HR-MS-Orbitrap), and their ecotoxicity was assessed with ECOSAR software, indicating they were less toxic than PXT. The T.E.S.T. software showed most TPs were not mutagenic but displayed developmental toxicity. Toxicity assessments from the pilot scale using the Microtox bioassay demonstrated that toxicity was eliminated by the end of the photocatalytic treatment. In conclusion, the study provides an integrative approach to photocatalytic degradation of PXT, integrating lab-scale and pilot-scale experiments, pure water and real WW matrices, environmentally relevant concentrations, TPs' identification along

with toxicity assessment of both *in-silico* and *in-vitro*, which is not followed in most previous studies dealing with the photocatalytic degradation of pollutants.

Keywords: Paroxetine, TiO_2, photocatalysis, wastewater, transformation products, CPC reactor

INTRODUCTION

Recent years' research on aquatic pollutants has focused on emerging contaminants (ECs) monitoring and decomposition into water ecosystems because it is a new group of chemical substances that are released continuously into the environment, mainly through WW, and many of them are considered persistent and carcinogenic, causing adverse effects on humans and animals' health[1,2].

A large share of aquatic ECs is "owned" by pharmaceutical active compounds (PhACs), as the pollution from these compounds has increased significantly over the years due to their high consumption[3,4]. It is estimated that 3,000 compounds are used as pharmaceutical products. However, more than 50% of all PhACs worldwide are not prescribed or dispensed legally, and many times, their intake is not indicated[4,5]. Therefore, the increasing use of pharmaceutical products implies the introduction of even tons of these compounds into the WW[6]. Such situations lead to the presence of PhACs in surface water and WW at concentrations ranging from a few ng/L to μg/L, considering them as "pseudo-persistent" pollutants even though they have relatively short half-lives in the environment[7,8]. Even at these trace concentrations, PhACs could be toxic to the environment and aquatic organisms[9].

Among PhACs, selective serotonin reuptake inhibitors (SSRIs) are the most prescribed worldwide and usually are the first choice for mental disorders treatment (e.g., depression)[10,11], but also for various medical purposes, including sleep and eating disorders, alcohol and drug abuse, panic, and post-traumatic stress disorders[12]. SSRIs should be chemically stable to induce a specific pharmacological response in the human body. However, this stability could potentially affect their removal from WW during treatment in conventional wastewater treatment plants (WWTPs). As a result, the appearance of the parent compounds or their transformation products (TPs) in treated WW and, consequently, in the natural aquatic environment is due to incomplete degradation[11].

Paroxetine (PXT) (CAS: 61869-08-7) [Supplementary Figure 1] is an SSRI approved for clinical use and has been available since the early 1990s. It is used for the treatment of clinical depression, obsessive-compulsive disorder, and panic disorder[10,13,14]. As a medicinal product, it is prescribed as hydrochloride salt[15].

In particular, PXT has been detected in several monitoring studies concerning the occurrence of PhACs in influents and effluents of WWTPs. Its removal in WWTPs varies from 30% to approximately 75%, indicating that it is not totally degraded[5,6,11,16-20]. PXT also has a tendency to adsorb onto activated sludge or other organic sediments during biological treatment in a conventional WWTP, thereby limiting its biodegradation[21]. PXT could be considered a "pseudo-persistent" contaminant as other antidepressant pharmaceuticals due to its potential presence in increased concentrations and its frequent appearance in the environment. Generally, antidepressant pharmaceuticals are grouped as pseudo-persistent pollutants of emerging concern[22]. The incomplete degradation of PXT in WWTPs has been noticed to induce spawning in zebra mussels at deficient concentrations of 10^{-7} M, equivalent to about 30 μg/L, according to toxicological studies[19], indicating potential adverse effects in the aquatic food chain, thus demonstrating the need for more efficient methods such as advanced oxidation processes (AOPs).

AOPs are characterized by their recent application in water decontamination without causing secondary pollution, while at the same time, they are promising, effective, environmentally friendly, and economically feasible techniques[23,24]. The common idea of AOPs is the *in situ* production of highly reactive species, for example, the hydroxyl radical (•OH) and the anionic superoxide radical ($•O_2^-$), which then non-selectively "attack" the organic pollutants to degrade them first into products of lower molecular weight and finally to mineralize them into non-toxic products such as H_2O, CO_2, and inorganic acids[25-27].

Heterogeneous photocatalysis has been proven a very promising AOP for organic pollutants' degradation because of its high performance, simplicity, reproducible results, and easy handling[28]. Plenty of semiconductors have been utilized as photocatalysts, but TiO_2 remains one the catalysts commonly used in "real-world" applications due to its excellent catalytic performance, low cost, excellent hydrophilicity, remarkable photostability, and non-toxicity[23,29-32]. Another aspect of TiO_2 is that it can be used in dispersed (slurry) or in thin film form (immobilized catalytic layer). When the catalyst is applied as a suspension, it has enough advantages; the most significant is the high photocatalytic performance[24,33].

Compound parabolic collectors (CPCs) are the photocatalytic reactor systems that prevail today. Some of their advantages are the collectors' parabolic geometry, which collects both direct and diffuse sunlight, reflecting it on the tube, a condition that enables CPCs to function during cloudy days, the absence of tracking systems, and the increased quantum yield when the photons' concentration is high[3,34-37]. Although TiO_2 has been widely used in pilot-scale applications for the degradation of organic pollutants, the studies focus on either the use of artificial light sources (e.g., LED lamps), which increase the operating costs, or on small WW volumes operated in batch mode, or specific water matrices, such as municipal WW. Additionally, most studies did not consider the reuse of the catalyst in the process in terms of its impact on performance[34,37-40].

Based on all the above, this work reveals new insights into the photocatalytic removal of PXT in water (lab scale) and secondary hospital wastewater (HWW) effluent (pilot scale) using a CPC photoreactor. TiO_2 P-25 catalyst is applied in three different concentrations to identify the optimal concentration for the fastest drug removal using simulated solar radiation for laboratory-scale experiments and natural sunlight for pilot-scale experiments. Furthermore, the study examined the extent of PXT's mineralization and the identification of its TPs while proposing a transformation pathway with this photocatalyst. The potential ecotoxicity and mutagenic properties of PXT and its TPs are determined by *in-silico* tools such as ECOSAR and toxicity estimation software tool (TEST) software. Compared to other studies on photocatalytic degradation of organic pollutants in an aqueous matrix, the present study provides an integrative approach, providing experimental data at both the lab scale and pilot scale. It examines degradation in pure water but also in real wastewaters (WW), at environmentally relevant concentrations, studying mineralization and TPs' formation with toxicity assessment both *in-silico* and *in-vitro*.

EXPERIMENTAL

Reagents, solvents, and materials

High-purity PXT (TCI, Zwijndrecht, Belgium) and commercial pharmaceutical product Seroxat (tablet containing 20 mg PXT, GlaxoSmithKline Pharmaceuticals S.A., Poznan, Poland) were used for lab-scale and pilot-scale experiments, respectively. Titanium dioxide (TiO_2) P-25 (average particle size: 30 nm, 80% anatase and 20% rutile, specific surface area 50 $m^2 \cdot g^{-1}$) was supplied by Evonik (Essen, Germany). Freeze-dried *Vibrio fischeri* bacterium in solid form (Acute Reagent) and a reconstitution solution used for its activation were supplied by Modern Water (New Castle, DE, USA). For the lab-prepared solutions, ultra-

pure water was used by an Evoqua apparatus (Pittsburgh, PA, USA), while for pilot-scale experiments, secondary effluent from the University Hospital of Ioannina City was used as a substrate, whose physicochemical parameters are listed in Supplementary Table 1 and studies about other ECs have already been conducted[5,41]. Further information is provided in the Supplementary Materials.

Lab-scale photocatalytic experiments

The lab-scale photocatalytic degradation of PXT took place in aqueous solution (10 mg/L, 200 mL) under simulated solar irradiation using a SUNTEST CPS+ apparatus (Atlas, Linsengericht, Germany). This simulator is equipped with a 1,500 W Xenon arc lamp and a glass filter permitting solar radiation within 300 to 800 nm. The lamp intensity was adjusted to 500 W/m^2, corresponding to a radiation dose of 150 kJ per 5 min of irradiation. PXT's aqueous solutions were irradiated in a 250 mL Duran glass Pyrex reactor under magnetic stirring. At the same time, tap water circulation cooled the reactor, so the temperature of the contained solution did not exceed 25 °C. The catalyst's concentration was adjusted to 200, 300, and 500 mg/L. After adding the catalyst, the suspension was left in the dark for 30 min to achieve the adsorption-desorption equilibrium of PXT on the catalyst's surface. Aliquots were taken at 0, 5, 15, 30, 45, 60, 90, 120, 180, 240, 300, and 360 min of the photocatalytic procedure, filtered through 0.22 μm PTFE syringe filters to remove the catalyst, and finally stored at dark conditions at 2-4 °C till immediate analysis.

Pilot-scale photocatalytic experiments

The photocatalytic experiments for PXT degradation at the pilot scale were carried out with a CPC reactor [Supplementary Figure 2] at the University Hospital of Ioannina (northwestern Greece) WWTP. This pilot reactor consists of collectors made of two aluminum half cylinders exposed to sunlight, a feed tank equipped with an air blower and an agitator, a recirculation pump, and a settling tank. Pipes connect the whole system and work in batch-recirculation mode. The CPC reactor consists of 24 borosilicate glass tubes (55 mm diameter × 1.5 m length, wall thickness 1.8 mm) with a total volume of 85 L, and its radiated surface is 12 m^2.

The experimental process began with filling the feed tank with secondary WW effluent from the WWTP of the University Hospital of Ioannina. The homogenization of the WW was carried out inside the feed tank with mechanical agitation and airflow from the air blower, which is located at the bottom of the tank. During homogenization, WW was spiked with an aqueous solution of the commercial antidepressant drug Seroxat. The spiked concentration of PXT was 20 μg/L. After spiking, homogenization continued for 15 min. Then, the catalyst was added, and the system was allowed to homogenize for another 15 min in the feed tank. The CPC reactor was then filled with the WW-catalysts suspension using the recirculation pump and remained under recirculation for 30 min while it was covered with a dark plastic cover to prevent any photoreaction before the start of the photocatalytic process. Then, the cover was removed so the photoreactions could take place, and samples were taken at predefined times. Each sample was filtered through PVDF Durapore membranes (0.45 μm) purchased from Merck (Carrigtwohill, Ireland) in a glass filtration device from MilliporeSigma (Massachusetts, USA) and kept at 4 °C till analysis.

The decrease in PXT concentration (C/C_0) in each photocatalytic experiment was observed as a function of a normalized illumination time (t_{30W}, min) and accumulated UV energy (Q_{UV}, kJ/L), as reported in previous studies[35,36,40], according to the following equations:

$$t_{30W,n} = t_{30W,n-1} + \frac{\bar{I}_{UV,n}}{30\ W/m^2} \times \frac{V_i}{V_t} \times \Delta t_n \quad \text{with } \Delta t_n = t_n - t_{n-1} \text{ and for } t_0 = 0\ (n = 1) \tag{1}$$

$$Q_{UV,n} = Q_{UV,n-1} + \Delta t_n \times \bar{I}_{UV,n} \times \frac{A_r}{V_t} \quad \text{with } \Delta t_n = t_n - t_{n-1} \tag{2}$$

where t_n is the experimental time (min) of treatment, V_i is the irradiated volume (L) of WW, V_t is the total volume (L) of WW, $I_{UV,n}$ is the average value of solar UV radiation (W/m^2) (λ = 300-400 nm) measured in the interval Δt, and A_r is the reactor's irradiated surface (m^2).

Analytical determinations

Determination of PXT residual concentration with HPLC

PXT concentration in the samples obtained from lab-scale experiments was determined by a Shimadzu (Kyoto, Japan) HPLC system consisting of a solvent delivery pump (LC-10AD), a degasser unit (DGU-14A), an auto-sampler (SIL-20A), a photodiode array detector (SPD-M10A), and a column oven (CTO-10A). The chromatographic column was a Discovery C18 (15 cm × 4.6 mm, 5 μm particle size) purchased from Supelco (Bellefonte, PA, USA). The injection volume was configured to 20 μL, utilizing a solvent mixture of 70:30 water and acetonitrile with 0.1% v/v Formic Acid as the mobile phase (isocratic elution). The mobile phase flow rate was set to 1 mL/min, with the column oven temperature maintained at 40 °C. The chromatograms were recorded using LabSolutions software. The retention time (R_t) of PXT was observed at 6.30 min.

Determination of mineralization degree by ion chromatography and total organic carbon analyzer

The concentration of F^-, NO_2^-, and NO_3^- anions in the photocatalytically treated samples was determined by a Shimadzu (Kyoto, Japan) ion chromatography system consisting of a solvent pump (LC-20Ai), a conductivity detector (CDD-10A), and a column oven (CTO-40C). The system is connected to a PC through the communication unit (CBM-40). The anion chromatography column was Shodex IC SI-35 4D (15 cm × 4.6 mm, 3.5 μm particle size) purchased from Showa Denko America (New York, USA). The injection volume was 20 μL, while the mobile phase, an aqueous Na_2CO_3 solution (3.6 mM), adjusted its flow to 0.6 mL/min. The column oven was set at 40 °C. The acquisition of the chromatograms and the processing of the results were carried out with the LabSolutions software.

A TOC-L automatic analyzer was utilized with an 8-place OCT-L autosampler from Shimadzu (Kyoto, Japan). First, every sample's total carbon load (TC) was determined through catalytic oxidation at 680 °C in an oxygen-rich environment. Afterward, the sample's inorganic carbon (IC) was determined, oxidating the carbonate ions contained in the sample in the presence of HCl (1 M). The CO_2 produced from both cases was measured through an NDIR detector. Finally, the total organic carbon (TOC) value is obtained by the equation: TOC = TC - IC. The results were obtained via PC-installed TOC Control-L software provided by Shimadzu.

Solid-phase extraction

The samples collected during the lab-scale photocatalytic experiments were subjected to solid-phase extraction (SPE) to pre-concentrate the TPs resulting from PXT degradation. The SPE process was carried out with the 4-position automatic SPE device from LabTech (Bergamo, Italy) connected to an air compressor from JUN-AIR (Norresundby, Denmark) and a laboratory nitrogen gas generator Alliance ALIZE-6/0 of Innovative Gas System Company (Evry, France). CHROMATific HLB+ micro-cartridges (60 mg, 3 mL) supplied by Chromatific (Heidenrod, Germany) were used. All SPE steps were performed by the SPE device automatically after being defined by the LabTech software. The protocol followed starts with conditioning the cartridges with 5 mL of methanol (LC-MS grade) and 5 mL of water (LC-MS grade). Then, the sample volume of 2 mL was loaded and extracted. The columns were then allowed to dry for 20 min under vacuum. The cartridges were eluted with 2 × 2.5 mL of methanol, and each sample's eluate was

collected in a 40 mL test tube. Afterward, the tubes were transferred to a Techne Dri-Block heater Model DB-3D (Staffordshire, United Kingdom), and samples were evaporated to dryness using a gentle stream of N_2 and heating (40 °C). Finally, each aliquot was reconstituted with 500 μL of methanol: water at a ratio of 2:98 v/v containing 0.1% v/v formic acid.

In the case of the pilot scale sample extraction, a protocol that has been previously reported[5,35] was followed. Before the SPE process, 100 mL of each sample was prepared by adjusting the pH to 7 and adding 2 mL of an aqueous Na_2EDTA 5% w/v solution. The addition of Na_2EDTA solution is because it complexes with metal ions, which are soluble in water and tend to form complexes with pharmaceutical compounds, reducing the extraction yield. The SPE was carried out using a Supelco (Bellefonte, PA, USA) Visiprep DL 12-place extraction apparatus connected to a Laboport (Oxfordshire, United Kingdom) vacuum pump. OASIS HLB cartridges (200 mg/6 mL) from Waters Corporation (Milford, MA, USA.) were used. The extraction procedure reported above was also followed.

Detection and identification of PXT and TPs by UHPLC-LTQ-Orbitrap

A UHPLC Accela LC system, connected with a hybrid LTQ-FT Orbitrap XL 2.5.5 SP1 mass spectrometer equipped with an electrospray ionization (ESI) source (Thermo Fisher Scientific, Inc., GmbH, Bremen, Germany) was used for the detection of PXT in pilot scale experiments and TPs in the treated samples. For the analysis of TPs, a full scan in positive ionization (PI) mode was applied within a mass range of 50-800 Da and a mass resolving power of 60,000 FWHM. In addition, a data-dependent acquisition (full MS/dd-MS^2) based on collision induced dissociation (CID) was carried out. More information about the operational parameters of the LTQ-FT Orbitrap instrumentation is listed in Supplementary Table 2. The chromatographic column used was a Hypersil Gold (100 mm × 2.1 mm, 1.9 μm particle size) from Thermo Fisher Scientific (Bremen, Germany). A mixture of water (solvent A) and methanol (solvent B) containing 0.1% v/v formic acid was used as a mobile phase. The elution gradient started with 98% solvent A (initial conditions) and remained for 2 min. Then, it progressed to 70% in 5 min and 50% in 10 min. The percentage of solvent A reached 2% after 15 min, returned to the initial conditions 10 s later, and remained like this until the end of the run. The total run time was 20 min. The injection volume was 10 μL, the flow of the mobile phase was adjusted to 350 μL/min, and the column's oven temperature was set at 35 °C. The chromatograms, mass spectra, and results processing were acquired with Xcalibur 2.1 software (Thermo Electron, San Jose, CA, USA).

Determination of secondary treated HWW physicochemical parameters

Conductivity was measured by an LF 325 portable conductometer purchased from WTW (Weilheim, Germany). Chemical oxygen demand (COD) was measured using the standard COD Cell Tests: C3/25 (10-150 mg/L) and C4/25 (25-1,500 mg/L), a thermoreactor CR 3200 and a WTW photo Flex photometer, all purchased from WTW (Weilheim, Germany). Five-day biochemical oxygen demand (BOD_5) was measured following a standard protocol from WTW (Weilheim, Germany) and using a WTW TS 606-G/2-i incubation cabinet and a WTW portable OxiTop OC 110 meter. The phenolic content of the samples was determined by the Folin-Ciocalteau method. The procedure started with mixing 5 mL of the sample and 250 μL of Folin-Ciocalteau reagent. After 2 min, 750 μL of Na_2CO_3 solution was added, and the mixture was left in the dark for 1 hour. Finally, the absorbance was measured at the wavelength of 750 nm using a UV-Vis spectrophotometer V-630 purchased from JASCO (Tokyo, Japan). The absorbance of the samples at 254 nm was measured to determine the content of aromatic compounds. Determination of chloride (Cl^-), nitrate (NO_3^-), and sulfate (SO_4^{2-}) ion concentrations in secondary treated HWW was performed by ion chromatography as described above.

In-silico ecotoxicity assessment and prediction of ecotoxicological values (mutagenicity, bioconcentration factor, and developmental toxicity)

The ecotoxicity of PXT and its TPs was assessed using the ECOSAR software (version 2.2). ECOSAR uses a large dataset (130 structural classes) of ecotoxicity studies from the ECOTOX database, following USEPA Office of Chemical Safety and Pollution Prevention guidelines. This software assesses the acute and chronic toxicity of chemical compounds to aquatic organisms using structure-activity relationship (SAR) models. The acute ecotoxicity assessment was calculated at three trophic levels: fish, daphnia (LC_{50} value), and green algae (EC_{50} value). Additionally, the chronic toxicity (ChV) values for the chemical compounds studied were calculated using the ECOSAR software.

The TEST software (version 5.1.2) was used to evaluate the potential for mutagenicity, developmental toxicity, and bioconcentration factors (BCFs) of PXT and its TPs. This software, like ECOSAR, was developed by the USEPA and uses QSAR models to make predictions. The consensus method was employed, which provides the most accurate predictions according to the user's guide.

RESULTS AND DISCUSSION

Photocatalytic degradation of PXT in lab-scale experiments

Studying the photocatalytic degradation of PXT (10 mg/L) in the laboratory showed that its complete degradation is possible within 45 min of irradiation with all three photocatalyst concentrations following pseudo-first-order kinetics [Figure 1A]. As can be observed from Supplementary Table 3, the higher the photocatalyst concentration, the faster the degradation of the pharmaceutical compound. The degree of PXT mineralization was also studied by determining the TOC concentration and F^-, NO_2^-, and NO_3^- anions. The determination coefficients obtained for each case (Supplementary Table 4, $R^2 > 0.9$) confirm that the pseudo-first-order kinetics model is also followed to a satisfactory degree for TOC decrease. Moreover, as seen in Figure 1B, increasing the catalyst's concentration leads to TOC's faster decrease. Specifically, in the case of applying 500 mg/L TiO_2, the TOC has decreased by approximately 95% after 360 min of irradiation; in the case of 300 mg/L TiO_2 by 86%, while in the case of 200 mg/L TiO_2, it has been decreased by 65%. Additionally, it is observed that in the first 60 min of each photocatalytic process (where PXT is not detected after 45 min), the concentration of TOC decreases relatively slowly, concluding that, during PXT's degradation, TPs are formed, which are further degraded, implying a decrease in TOC.

Secondly, the mineralization degree was studied by monitoring the F^-, NO_2^-, and NO_3^- concentrations. The maximum concentrations that can be stoichiometrically derived from the complete oxidation of PXT (10 mg/L) are $[F^-]_{st}$ = 0.577 mg/L, $[NO_2^-]_{st}$ = 1.397 mg/L, and $[NO_3^-]_{st}$ = 1.883 mg/L.

Comparing the evolution kinetics of fluorine anions for the three catalyst concentrations applied [Figure 2A], a rapid increase in their concentration is observed in the first 45 min of each photocatalytic process. Accordingly, PXT has been completely removed at this time, which causes the rapid release of fluorine ions. From 45 to 360 min, the concentration remains almost unchanged. Worthy of attention is the case of using 200 mg/L TiO_2, where the concentration of fluorine ions formed is higher than those derived from the other catalyst concentrations studied. Theoretically, it would be expected that the higher the catalyst concentration, the higher the release rate of fluorine ions in the solution due to the advanced and faster degradation of the parent compound containing fluorine atoms in its structure. However, after 360 min of irradiation using 200 mg/L TiO_2, F^- released corresponded to 63% of the stoichiometrically derived concentration, while when using 300 and 500 mg/L catalyst concentrations, the relative percentage becomes approximately 36% and 47%, respectively. An explanation for this phenomenon can be given by the tendency of fluorine ions to adsorb on the surface of TiO_2, as has been reported in the literature[42]. In particular, the pH of the solution is one of the conditions that favor the adsorption of fluorine ions on the

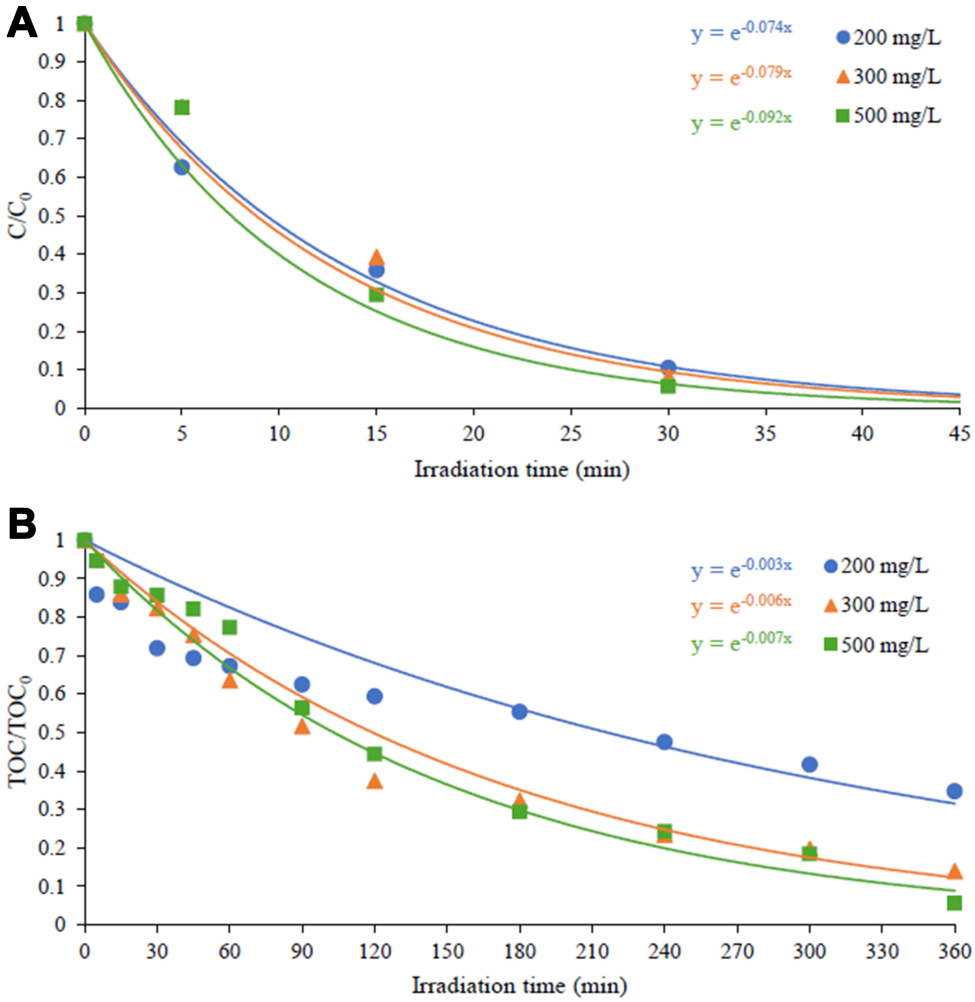

Figure 1. (A) Degradation kinetics of PXT (C_0 = 10 mg/L) and (B) TOC decrease kinetics with TiO_2 P-25 catalyst (200, 300, and 500 mg/L) under simulated solar irradiation (I = 500 W/m^2). PXT: Paroxetine; TOC: total organic carbon.

catalyst's surface. In addition, the amount of catalyst in the solution plays an important role. On the one hand, a high catalyst concentration implies faster photocatalytic degradation and release of fluorine ions in the solution. On the other hand, a high concentration (up to an optimum point) implies the adsorption of the ions on the catalyst surface.

Regarding the transformation of piperidine-nitrogen heteroatom, no NO_2^- ions were detected in any samples, regardless of the catalyst concentration. This could be due to their immediate oxidation to NO_3^- after their production because of the abundance of hydroxyl radicals in the solution. The evolution kinetics of NO_3^-, as shown in Figure 2B, is "driven" by the concentration of the catalyst. That is, the greater the concentration of the catalyst, the greater the concentration of nitrate ions that appear at any time. The evolution kinetics for nitrate ions appears to have a similar pattern in all three catalyst concentration cases. Specifically, after a sharp increase within the first 15 min of irradiation, the concentration increases at a slower rate of up to 90 min, followed by a second step of higher formation slope up to 180 min (more intense at catalyst concentrations of 200 and 300 mg/L), and then a further gentle increase up to 360 min.

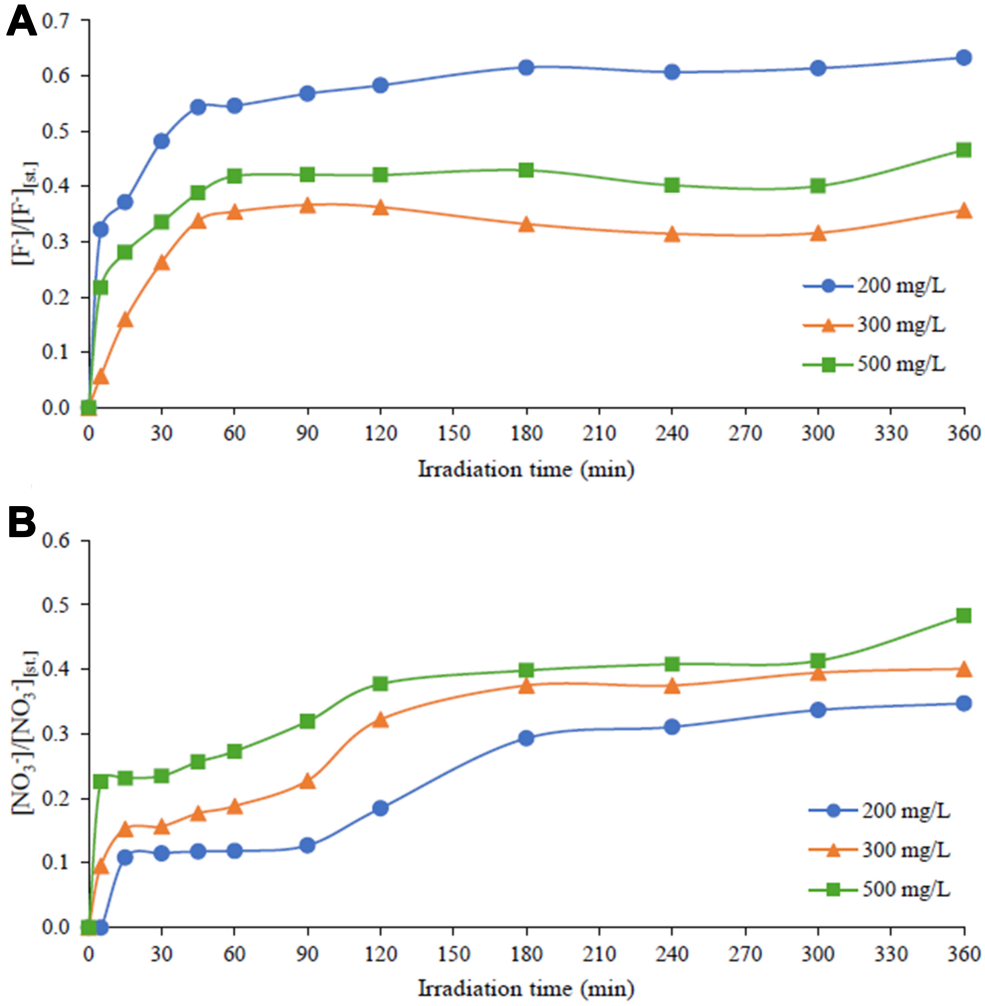

Figure 2. Evolution kinetics of the produced F^- (A) and NO_3^- (B) anions during the photocatalytic degradation of PXT with TiO_2. PXT: Paroxetine.

This increase in NO_3^- concentration in two distinct steps can be associated with the formation of intermediate compounds, which can undergo further reactions, leading to the stepwise release of nitrogen. The first release step (0-15 min) in Figure 2B is most likely due to the degradation of the parent PXT molecule by oxidant species produced by TiO_2 photocatalysts. Subsequently, the second release step (60-180 min), which occurs at a lower rate, is most likely due to the release and oxidation of the nitrogen atoms from the TPs, also taking into account their evolutionary profiles presenting slower degradation of TP-208, TP-210, TP-226, and TP-296.

Thus, at the end of the photocatalytic process, for the concentration of 200 mg/L TiO_2, the concentration of NO_3^- corresponds to approximately 35% of the stoichiometrically available nitrogen, for the concentration of 300 mg/L, it corresponds to 40%, and for the concentration of 500 mg/L, it is approximately 48%.

Detection and identification of the photocatalytically produced TPs with TiO_2 P-25

Thirteen TPs were identified during the photocatalytic processes [Figure 3], and the data obtained from the processing of the chromatograms are shown in Table 1. The primary TP observed was TP-210 with a molecular formula of $C_{12}H_{17}ONF$. TP-210 appeared at 5.44 min and was formed by removing the

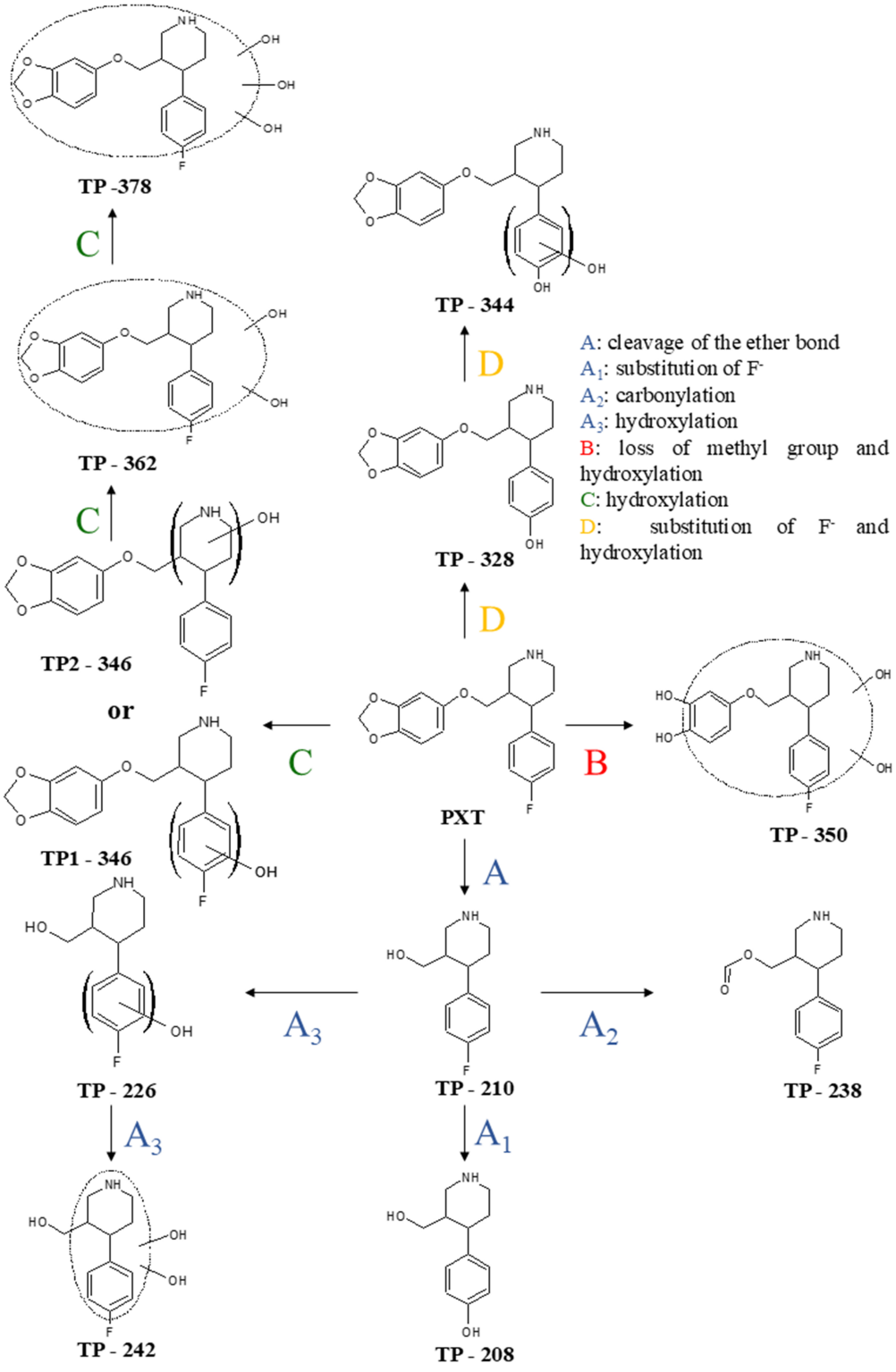

Figure 3. Proposed pathway for the photocatalytic transformation of PXT with TiO_2 P-25. PXT: Paroxetine.

benzodioxol part from the PXT molecule, with a mass difference of 120.0203 Da. Its structure was determined by analyzing MS^2 fragments with *m/z* values of 192.1178, 163.0912, 123.0599, and 109.0444,

Table 1. High-resolution mass data of PXT and its TPs formed during the photolytic and photocatalytic degradation experiments

Compound	R_t (min)	$[M+H]^+$	Molecular formula	Δ (ppm)	RDB	MS^2 $[M+H]^+$	Molecular formula	Δ (ppm)	RDB
PXT	11.29	330.1491	$C_{19}H_{21}O_3NF$	-2.993	9.5	313.1228	$C_{19}H_{18}O_3F$	-2.073	10.5
						192.1178	$C_{12}H_{15}NF$	-2.416	5.5
						178.1022	$C_{11}H_{13}NF$	-2.550	5.5
						163.0914	$C_{11}H_{12}F$	-2.300	5.5
						151.0386	$C_8H_7O_3$	-2.189	5.5
						123.0599	C_8H_8F	-4.917	4.5
						109.0443	C_7H_6F	-4.631	4.5
TP-208	1.58	208.1328	$C_{12}H_{18}O_2N$	-1.515	4.5	190.1222	$C_{12}H_{16}ON$	-2.370	5.5
						161.0958	$C_{11}H_{13}O$	-1.872	5.5
						147.0799	$C_{10}H_{11}O$	-3.478	5.5
						121.0641	C_8H_9O	-5.712	4.5
						107.0482	C_7H_7O	-9.075	4.5
TP-210	5.44	210.1288	$C_{12}H_{17}ONF$	-0.994	4.5	192.1178	$C_{12}H_{15}NF$	-2.469	5.5
						163.0912	$C_{11}H_{12}F$	-3.220	5.5
						135.0595	C_9H_8F	-6.923	5.5
						123.0599	C_8H_8F	-4.673	4.5
						109.0444	C_7H_6F	-3.897	4.5
TP-226	4.69	226.1231	$C_{12}H_{17}O_2NF$	-2.979	4.5	208.1129	$C_{12}H_{15}ONF$	-1.292	5.5
						191.0862	$C_{12}H_{12}OF$	-2.301	6.5
						179.0862	$C_{11}H_{12}OF$	-2.791	5.5
						177.0706	$C_{11}H_{10}OF$	-2.370	6.5
						166.0661	C_9H_9ONF	-0.895	5.5
						165.0707	$C_{10}H_{10}OF$	-2.240	5.5
						163.0552	$C_{10}H_8OF$	-0.918	6.5
						139.0549	C_8H_8OF	-3.377	4.5
						125.0393	C_7H_6OF	-3.675	4.5
TP-238	9.55	238.1229	$C_{13}H_{17}O_2NF$	-3.458	5.5	-	-	-	-
TP-242	4.10	242.1181	$C_{12}H_{17}O_3NF$	-3.420	4.5	-	-	-	-
TP-296	6.45	296.1284	$C_{15}H_{19}O_4NF$	-2.542	6.5	278.1181	$C_{15}H_{17}O_3NF$	-2.258	7.5
						210.1287	$C_{12}H_{17}ONF$	-0.899	4.5
						192.1180	$C_{12}H_{15}NF$	-1.740	5.5
						190.1019	$C_{12}H_{13}NF$	-3.809	6.5
						163.0911	$C_{11}H_{12}F$	-3.833	5.5
						123.0600	C_8H_8F	-4.023	4.5
TP-328	7.84	328.1537	$C_{19}H_{22}O_4N$	-3.456	9.5	311.1272	$C_{19}H_{19}O_4$	-1.786	10.5
						298.1424	$C_{18}H_{20}O_3N$	-4.729	9.5
						281.1167	$C_{18}H_{17}O_3$	-1.853	10.5
						234.1120	$C_{13}H_{16}O_3N$	-1.794	6.5
						217.0854	$C_{13}H_{13}O_3$	-2.537	7.5
						206.1169	$C_{12}H_{16}O_2N$	-3.034	5.5
						190.1222	$C_{12}H_{16}ON$	-2.370	5.5
						173.0957	$C_{12}H_{13}O$	-2.147	6.5
						151.0386	$C_8H_7O_3$	-2.321	5.5
TP-344	7.00	344.1485	$C_{19}H_{22}O_5N$	-2.177	9.5	327.1220	$C_{19}H_{19}O_5$	-2.202	10.5
						314.1362	$C_{18}H_{20}O_4N$	-7.814	9.5
						234.1121	$C_{13}H_{13}O_3N$	-1.409	6.5
						217.0853	$C_{13}H_{13}O_3$	-2.675	7.5
						206.1172	$C_{12}H_{16}O_2N$	-1.481	5.5
						189.0908	$C_{12}H_{13}O_2$	-1.302	6.5
						177.0907	$C_{11}H_{13}O_2$	-1.729	5.5
						163.0750	$C_{10}H_{11}O_2$	-2.306	5.5
						151.0387	$C_8H_7O_3$	-1.924	5.5
						123.0435	$C_7H_7O_2$	-4.194	4.5
TP1-346	10.31	346.1441	$C_{19}H_{21}O_4NF$	-2.608	9.5	329.1179	$C_{19}H_{18}O_4F$	-1.439	10.5
						234.1121	$C_{13}H_{16}O_3N$	-1.623	6.5
						208.1129	$C_{12}H_{15}ONF$	-1.388	5.5
						194.0968	$C_{11}H_{13}ONF$	-3.961	5.5
						179.0863	$C_{11}H_{12}OF$	-1.897	5.5
						151.0387	$C_8H_7O_3$	-1.725	5.5
						139.0550	C_8H_8OF	-2.730	4.5
						125.0393	C_7H_6OF	-3.116	4.5
TP2-346	12.06	346.1440	$C_{19}H_{21}O_4NF$	-2.146	9.5	328.1339	$C_{19}H_{19}O_3NF$	-1.427	10.5
						208.1129	$C_{12}H_{15}ONF$	-1.292	5.5
						178.1024	$C_{11}H_{13}NF$	-1.427	5.5
						163.0915	$C_{11}H_{12}OF$	-1.897	5.5
						151.0386	$C_8H_7O_3$	-2.189	5.5
						109.0440	C_7H_6F	-7.199	4.5

TP-350	8.36	350.1392	$C_{18}H_{21}O_5NF$	-0.078	8.5	332.1286	$C_{18}H_{19}O_4NF$	-2.086	9.5
						306.1492	$C_{17}H_{21}O_3NF$	-2.607	7.5
						290.1184	$C_{16}H_{17}O_3NF$	-0.993	8.5
						210.1287	$C_{12}H_{17}ONF$	-0.613	4.5
						192.1180	$C_{12}H_{15}NF$	-1.844	5.5
						190.1025	$C_{12}H_{13}NF$	-1.022	6.5
						178.1027	$C_{11}H_{13}NF$	0.145	5.5
						163.0916	$C_{11}H_{12}F$	-1.074	5.5
						135.0597	C_9H_8F	-5.516	5.5
						123.0601	C_8H_8F	-3.048	4.5
TP-362	9.98	362.1388	$C_{19}H_{21}O_5NF$	1.194	9.5	-	-	-	-
TP-378	8.06	378.1337	$C_{19}H_{21}O_6NF$	-3.734	7.5	348.1234	$C_{18}H_{19}O_5NF$	-2.377	9.5
						334.1442	$C_{18}H_{21}O_4NF$	-2.223	8.5
						210.1284	$C_{12}H_{17}ONF$	-2.089	4.5
						192.1178	$C_{12}H_{15}NF$	-2.729	5.5

PXT: Paroxetine; TPs: transformation products; R_t: retention time; RDB: ring double-bond equivalents.

characteristic of the parent compound's molecule. Additionally, it should be noted this particular TP has been documented previously in the photolytic degradation of PXT[13,14].

TP-208 differs from TP-210 by 1.9960 Da and has the molecular formula $C_{12}H_{18}O_2N$ and can be rationalized by the substitution of the fluorine atom in the benzene ring with a hydroxyl group. This is supported by the fragments with *m/z* = 121.0641 and *m/z* = 107.0482, which differ by approximately 2 Da from the corresponding fragments of TP-210 (*m/z* = 123.0599 and *m/z* = 109.0444), as well as their molecular formulas. Thus, it has been verified that the hydroxyl group is positioned in the benzene ring, substituting fluorine.

TP-226 was observed eluting at 4.69 min. Its molecular formula is $C_{12}H_{17}O_2NF$, which differs from the molecular formula of TP-210 by 15.9943 Da, suggesting a hydroxylated derivative of TP-210. The additional hydroxyl group is positioned in the benzene ring, as indicated by MS^2 fragments with *m/z* = 139.0549 and *m/z* = 125.0393 and molecular formulas C_8H_8OF and C_7H_6OF, respectively. The corresponding fragments without the addition of oxygen are also present in the parent compound with *m/z* = 123.0599 and *m/z* = 109.0443 and molecular formulas C_8H_8F and C_7H_6F, respectively.

TP-296 was identified as having the molecular formula $C_{15}H_{19}O_4NF$. The MS^2 fragments characteristic of PXT consist of *m/z* = 192.1180, *m/z* = 163.0911, and *m/z* = 123.0600. The proposed molecular formula for TP-210 matches the fragment with *m/z* = 210.1287. For the fragment with *m/z* = 278.1181, the molecular formula $C_{15}H_{17}O_3NF$ was suggested. Despite obtaining sufficient information from the MS^2 fragments, a chemical formula for TP-296 cannot be determined, and it does not come to an agreement with the literature suggesting $C_{19}H_{19}ONF$ as the molecular formula of TP-296[13].

TP-328, with *m/z* = 328.1537, corresponds to a molecular formula of $C_{19}H_{22}O_4N$. The TP appears to result from replacing a fluorine atom in the PXT molecule with a hydroxyl group, similar to when TP-208 was created from TP-210. The fragment with *m/z* = 190.1222 and a molecular formula of $C_{12}H_{16}ON$ is the same as that reported for TP-208, indicating the hydroxyl group is located in the benzene ring. A fragment with *m/z* = 151.0386 and a molecular formula of $C_8H_7O_3$, which contains the benzodioxol moiety also found in the PXT molecule, was also detected (could be called a methoxy-benzodioxol structure). This fragment originated from the ether bond cleavage and includes three of the four oxygen atoms present in the TP. The substitution of fluorine in the benzene ring was confirmed by fragments with *m/z* = 234.1120 and *m/z* = 217.0854, resulting from the cleavage of the bond between the benzene and piperidine ring. These fragment ions contain three oxygen atoms, suggesting that the fourth oxygen atom will be found in the benzene ring.

TP-344 results from the addition of an oxygen atom to the structure of TP-328 as shown by the mass difference of 15.9948 Da between them, but also by the shorter retention time of TP-344 (7.00 min) than TP-328 (7.84 min), a fact showing that the former is a more polar molecule than the latter. Molecular structure identification was based on MS^2 fragment ions. Specifically, four common fragments with TP-328 are identified, with *m/z* values of 234.1121, 217.0853, 206.1172, and 151.0387. The first two (234.1121 and 217.0853) come from the cleavage of the bond between the benzene ring and the piperidine ring. From the piperidine ring, the nitrogen atom has also been removed as ammonia by the opening of the ring and its rearrangement to form a double bond. Thus, the difference of 17.0268 Da between the two fragments is also justified. Furthermore, a fundamental observation is that three of the five oxygen atoms in the molecular formula of the given TP are located in the molecular formula of these two fragments, which means that the remaining two oxygen atoms are located in the structure corresponding to TP-210. This observation is supported by the common fragment with *m/z* = 151.0387 having a methoxy-benzodioxol moiety (the three oxygen atoms are detected). It has resulted from the cleavage of the ether bond between the oxygen and the methyl carbon of the piperidine ring. Although the fragment with *m/z* = 206.1172 has the same molecular formula as the corresponding fragment of TP-328, it has a different structure. This concludes from the fragment with *m/z* = 123.0435, which indicates the existence of two hydroxyl groups on the benzene ring, which is connected to the piperidine ring. Therefore, since one hydroxyl group has replaced the fluorine atom in the PXT molecule, the second one will be located either in the o-position or in the m-position, with the o-position having more chances due to the activation of the benzene ring by the hydroxyl group present.

TP-346 is detected at two retention times in the chromatogram, at 10.31 and 12.06 min, considering that this particular TP presents two isomers. It was assigned the molecular formula $C_{19}H_{21}O_4NF$, confirming the addition of an oxygen atom to the PXT molecule, as indicated by a difference of 15.9950 Da. The structure for each isomer was identified by MS^2 data, aiming to find the location of the added hydroxyl group on the PXT molecule. In both TPs, the fragment with *m/z* = 151.0387 and molecular formula $C_8H_7O_3$ is detected, which has also been detected in the MS^2 spectrum for TP-328 and is the methoxy-benzodioxol moiety contained in the PXT molecule. As mentioned, three of the four oxygen atoms that the two isomers of TP-346 have are located in this structure. Therefore, the added hydroxyl group could be in the piperidine or benzene rings. From the fragment ions obtained for the first isomer (TP1-346) and, more specifically, the one with *m/z* = 125.0393 and a molecular formula C_7H_6OF, it is indicated that the hydroxyl group is located in the benzene ring with the most likely addition positions being o- position to fluorine.

The same finding has been made in the TP-226. On the contrary, for the second isomer (TP2-346), a fragment with *m/z* = 109.0440 and a molecular formula of C_7H_6F was obtained, meaning that the oxygen atom is not located in the benzene ring. Still, the moiety of the molecule where the hydroxyl group can be located is in the piperidine ring, following the previous finding for the fragment with *m/z* = 151.0837.

TP-350 with *m/z* = 350.1392 corresponds to the molecular formula $C_{18}H_{21}O_5NF$. This compound appears to be created by bi-hydroxylation in the PXT molecule and the five-membered ring's concurrent opening. The hydroxylated character is also denoted by the characteristic loss of H_2O (18.0106 Da), presenting a fragment ion with *m/z* equal to 332.1286. A fragment ion with an *m/z* value of 306.1492 is formed due to the loss of a CO_2 molecule (43.9900 Da)[13]. When trying to identify the additional hydroxyl groups on the molecule, characteristic fragment ions found in PXT were observed (*m/z* = 192.1180, *m/z* = 187.1027, *m/z* = 163.0916, and *m/z* = 123.0601). Moreover, the fragment ion with *m/z* = 210.1287 has the same structure as the TP-210, indicating that one of the five oxygen atoms in the molecule is located in this structure. Consequently, it is suggested that the two additional hydroxyl groups are positioned in the benzene ring of the benzodioxol moiety. However, due to steric effects, it is challenging to pinpoint both added hydroxyl groups in the

mentioned ring, as their simultaneous inclusion likely led to the ring's opening.

TP-378 eluted at 8.06 min and was assigned to the molecular formula $C_{19}H_{21}O_6NF$. It is considered adding three oxygen atoms (3 × 15.9949 Da) to the PXT molecule, most likely in hydroxyl groups. Two characteristic fragments were detected in the MS^2 spectrum, which is also detected for PXT having m/z = 210.1284 and m/z = 192.1178 and molecular formulas $C_{12}H_{17}ONF$ and $C_{12}H_{15}NF$, respectively. Two other fragment ions were detected with m/z = 348.1234 (molecular formula: $C_{18}H_{19}O_5NF$) and with m/z = 334.1442 (molecular formula: $C_{18}H_{21}O_4NF$), which cannot indicate the positions of the hydroxyl groups on the molecule's structure. Therefore, the only conclusion that can be drawn, and indeed not with absolute certainty, is that the specific TP is a tris-hydroxylated PXT molecule.

Finally, MS^2 data were not obtained for TP-238, TP-242, and TP-362 with molecular ions m/z = 238.1229, m/z = 242.1181, and m/z = 362.1388, respectively. However, their identification was possible considering their molecular type, retention time, and evolutionary profiles, indicating that these chemical structures did not pre-exist but were formed during the degradation of the parent compound; their concentration reached a maximum, and over time, they were also degraded. In particular, TP-238 with a molecular formula of $C_{13}H_{17}O_2NF$ was eluted at 9.55 min, and compared to the molecular formula of TP-210, one oxygen atom and one carbon atom were added. So, it is a carbonylated form of TP-210, as has been suggested in the literature[13].

TP-242 with molecular formula $C_{12}H_{17}O_3NF$ probably originates from the addition of an oxygen atom to TP-226 (the difference between them is equal to 15.9951 Da). Additionally, TP-242 elutes earlier (4.10 min) than TP-226 (4.69 min), an observation that confirms the more polar character of TP-242. However, the absence of fragment ions does not allow its precise identification. Accordingly, TP-362 (molecular formula $C_{19}H_{21}O_5NF$) differs from TP-346 by 15.9947 Da, and by extension, an oxygen atom has been added to the molecule of TP-346. TP-362, as a more polar molecule, elutes earlier than TP-346.

In summary, various primary and secondary hydroxylated products were consistently formed with the well-known potential of TiO_2 for hydroxyl radical generation, suggesting hydroxylation pathways as the major ones for PXT transformation.

The evolutionary profiles of the TPs are presented in Figure 4, showing that after 90 min of irradiation, regardless of the concentration of the photocatalyst, most of them have either been completely degraded or are presented in small amounts, such as TP-208, TP-210, and TP-226 until their complete degradation. This observation agrees with the TOC results, where after 90 min, the rate of its decrease becomes faster. TP-210 appears to be the most "resistant" to degradation, as regardless of the catalyst's concentration, it is no longer detected after 360 min. Finally, the maximum concentration of each TP (at 15 or 30 min of irradiation), especially in the case of the most hydroxylated products (TP-208, TP-226, TP-242, TP-362, TP-378), occurred when the catalyst concentration was the highest due to the higher production of hydroxyl radicals.

In-silico ecotoxicity assessment (lab-scale experiments)

Table 2 shows the theoretical acute (LC_{50}, EC_{50}) and chronic toxicity (ChV) values of PXT and its TPs for fish, daphnids, and green algae. The Globally Harmonized System of Classification and Labelling of Chemicals (GHS) was used. For TPs with undetermined functional groups, the average toxicity, mutagenicity, and BCF values were calculated by placing the functional group at each possible position on the molecule. Furthermore, no definitive conclusion can be drawn about the ecotoxicity of TP-296 due to the inability to suggest its molecular formula and the TEST software's incapability to calculate mutagenicity

Table 2. *In-silico* assessment of acute and chronic toxicity of PXT and its TPs with ECOSAR v2.2 software (chemical category: aliphatic amins)

Compound	Acute toxicity (LC_{50}/EC_{50})			Chronic toxicity (ChV)		
	Fish LC_{50} (mg/L)	Daphnid LC_{50} (mg/L)	Green algae EC_{50} (mg/L)	Fish ChV (mg/L)	Daphnid ChV (mg/L)	Green algae ChV (mg/L)
PXT	3.29[b]	0.493[a]	0.259[a]	0.096[a]	0.050[a]	0.101[a]
TP-208	116[d]	12.7[c]	12.3[c]	8.64[b]	0.963[a]	3.86[b]
TP-210	41.7[c]	4.96[b]	4.11[b]	2.45[b]	0.406[a]	1.36[b]
TP-226	92.8[c]	10.4[c]	9.67[b]	6.46[b]	0.810[a]	3.08[b]
TP-238	23.6[c]	2.96[b]	2.21[b]	1.18[b]	0.256[a]	0.762[a]
TP-242	1,355.4[d]	121.6[d]	176.3[d]	190[d]	7.61[b]	47.6[c]
TP-328	2.77[b]	0.420[a]	0.216[a]	0.078[a]	0.044[a]	0.085[a]
TP-344	6.01[b]	0.862[a]	0.494[a]	0.200[a]	0.085[a]	0.187[a]
TP1-346	2.16[b]	0.335[a]	0.164[a]	0.056[a]	0.036[a]	0.066[a]
TP2-346	10.7[c]	1.47[b]	0.918[a]	0.407[a]	0.138[a]	0.337[a]
TP-350	16.5[c]	2.19[b]	1.46[b]	0.692[a]	0.200[a]	0.524[a]
TP-362	28.0[c]	3.50[b]	2.63[b]	1.42[b]	0.303[a]	0.901[a]
TP-378	11.14[c]	5.39[b]	4.53[b]	2.45[b]	0.453[a]	1.44[b]

[a]Very toxic (LC_{50}/EC_{50}/ChV < 1 mg/L); [b]Toxic (1 mg/L < LC_{50}/EC_{50}/ChV < 10 mg/L); [c]Harmful (10 mg/L < LC_{50}/EC_{50}/ChV < 100 mg/L); [d]Not harmful (LC_{50}/EC_{50}/ChV > 100 mg/L). PXT: Paroxetine; TPs: transformation products.

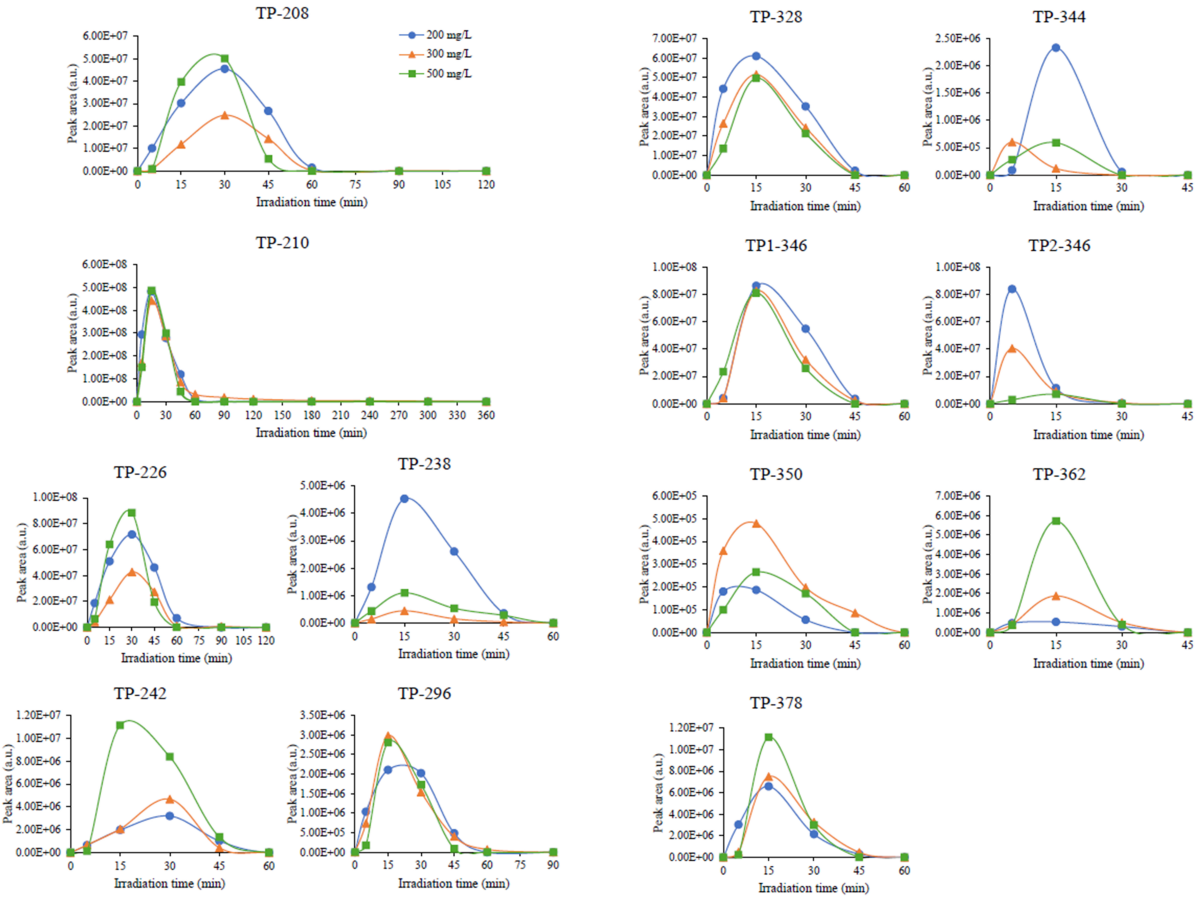

Figure 4. Evolutionary profiles of each TP detected in photocatalysis with TiO_2 P-25 in concentrations 200, 300, and 500 mg/L. TP: Transformation product.

and BCF values for TP-238.

The summarized data show that PXT is highly toxic to daphnids and green algae. Regarding fish, PXT is toxic after brief exposure and highly toxic in chronic exposure. For the TPs, TP-208 and TP-242 were identified as non-harmful to fish in short exposure, and TP-242 continued to be non-harmful during chronic exposure. In general, the majority of TPs detected are either highly toxic or toxic to the aquatic organisms mentioned above during both short and long-term exposure.

The high toxicity of PXT has been confirmed by *in-vitro* studies on various microalgae species, including *Scenedesmus rubescens*, *Chlorococcum sp*., and *Dunaliella tertiolecta* algae, which play an essential role as aquatic producers. PXT notably impacts algal growth within the first 24 h, with some instances showing complete inhibition of growth rates at 100%. Possibly, the acute ecotoxicity of PXT on algae relates to its chemical structure, particularly the aromatic ring and amino group, which may interact with the biological membranes of microorganisms[43]. Additionally, other studies examined the toxicity of PXT metabolites excreted from the human body, but these products were not detected in the present study[44,45]. Thus, the available studies in the literature do not address the potential impact of the detected PXT's TPs on different organisms. It is known that in aquatic environments, particularly at lower trophic levels (e.g., microalgae), population reductions caused by toxic compounds directly affect the subsequent trophic level (e.g., green microalgae are consumed by daphnids). Therefore, the presence of PXT's TPs may have potential effects on aquatic food chains.

Determining toxicological risk due to potential harm and carcinogenicity is crucial to assessing mutagenicity. QSAR models are utilized to predict the mutagenicity of new or data-lacking chemicals[46,47]. It has been established that PXT does not possess mutagenic potential. From Figure 5, it has been observed that TPs that could cause mutagenic reactions are TP-210 and TP-226. To address the formation of these specific TPs during photoinduced processes, their evolutionary profiles are considered, where complete degradation is observed, producing non-mutagenic compounds.

When assessing chemical pollutants, it is crucial to also consider their BCF, which indicates their potential to accumulate in organisms in aquatic environments. Modeling BCF is often done due to challenges in conducting experiments for many pollutants[48,49]. Predicted BCF values suggest that PXT's TPs are less likely to accumulate in aquatic organisms than the parent compound, indicating a lower potential for harmful effects.

Regarding developmental toxicity, the TEST software classified both PXT and all the TPs formed as "developmental toxicant" as the predicted values for all compounds are > 0.5. TP1-346, TP2-346, and TP-362 were much more "developmental toxicant" than PXT. Although this may be concerning, considering the evolutionary profiles of the corresponding TPs, it is evident that after 60 min of the photocatalytic process, regardless of the photocatalyst concentration, the TPs are completely degraded.

Photocatalytic degradation of PXT in pilot-scale experiments and environmentally relevant concentration levels

The photocatalytic degradation of PXT (20 μg/L) was studied with a CPC pilot reactor under natural solar irradiation and TiO_2 photocatalyst. Figure 6A presents the data from the photocatalytic degradation of PXT as a function of the accumulated UV energy per liter of WW (Q_{UV}), while Figure 6B presents the same data as a function of a normalized illumination time (t_{30W}). PXT's degradation kinetics follows a pseudo-first-order model, as in lab-scale experiments. From the data in Table 3, PXT's removal from WW was satisfying,

Table 3. Pseudo-first-order rate constant (k_{app}), correlation coefficient (R^2), and % removal of PXT after pilot-scale photocatalytic treatment

TiO_2 P-25	PXT (20 μg/L)		
C (mg/L)	k_{app} (L/kJ)	R^2	%
200	0.05	0.9213	92
300	0.034	0.9219	79
500	0.039	0.9268	76

PXT: Paroxetine.

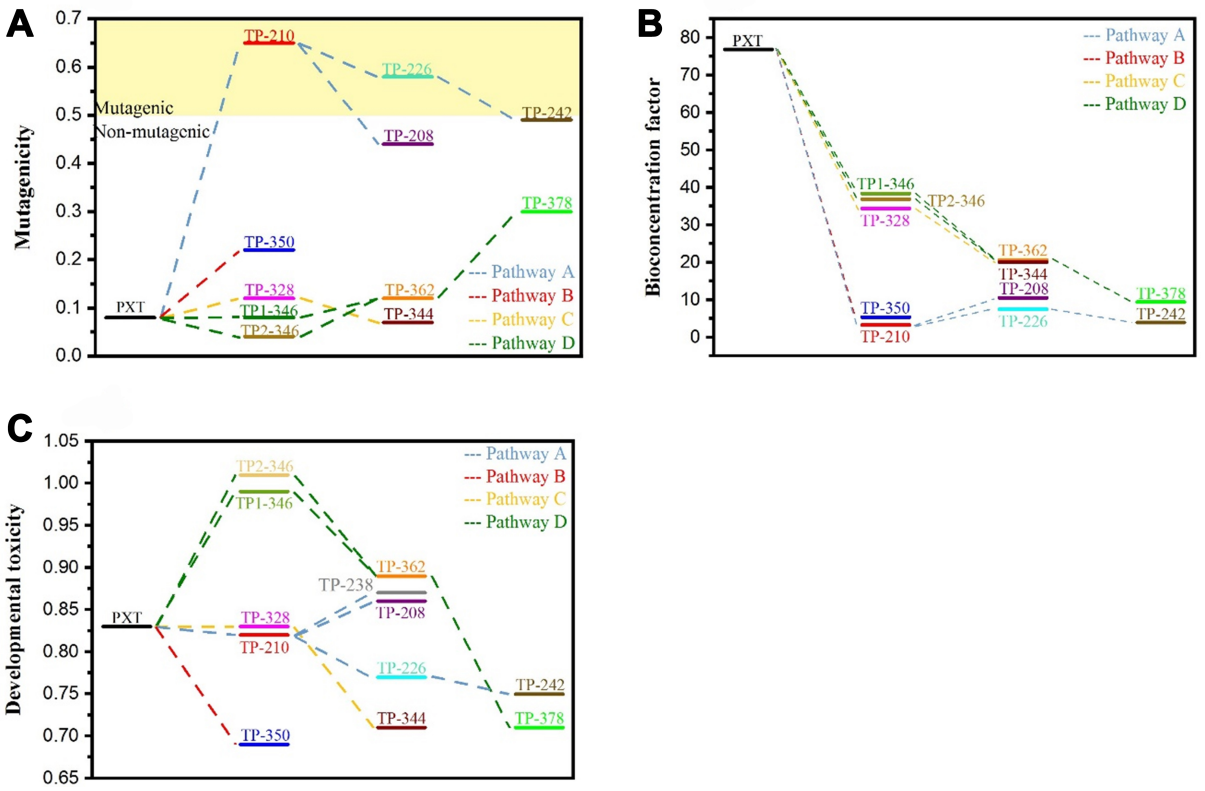

Figure 5. *In silico* predicted values for (A) mutagenicity, (B) BCF, and (C) developmental toxicity of PXT and its TPs formed during photocatalysis with TiO_2 P-25. BCF: Bioconcentration factor; PXT: Paroxetine; TPs: transformation products.

ranging from 76% to 92%. Also noteworthy is that in the case of the 200 mg/L photocatalyst concentration, removal was achieved faster (k = 0.05 L/kJ) than the other two photocatalyst concentrations and the highest removal was achieved (92%).

In contrast to the lab-scale photocatalytic experiments, it was reported that the higher the photocatalyst concentration, the faster the degradation of the pharmaceutical compound was, whereas this condition was not followed. This can be observed in Figure 6A, where Q_{UV} values are greater at the exact sampling times in the case of photocatalysis with 200 mg/L TiO_2.

Additionally, the concentration of 200 mg/L is presented as the optimal catalyst concentration for this pharmaceutical's removal compared to the other two catalyst concentrations (300 and 500 mg/L). It thus ensures the effective absorption of photons from the catalyst, as referred to in other case studies[35,50]. When

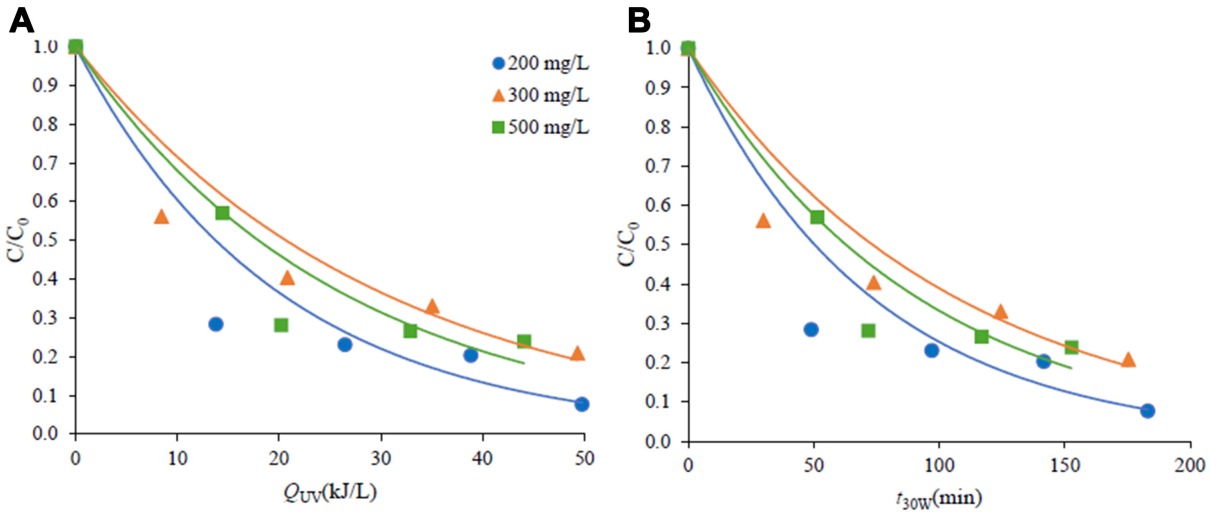

Figure 6. Degradation kinetics of PXT (C_0 = 20 μg/L) with TiO_2 P-25 catalyst (200, 300, and 500 mg/L) under natural solar irradiation as a function of Q_{UV} (A) and t_{30W} (B). PXT: Paroxetine.

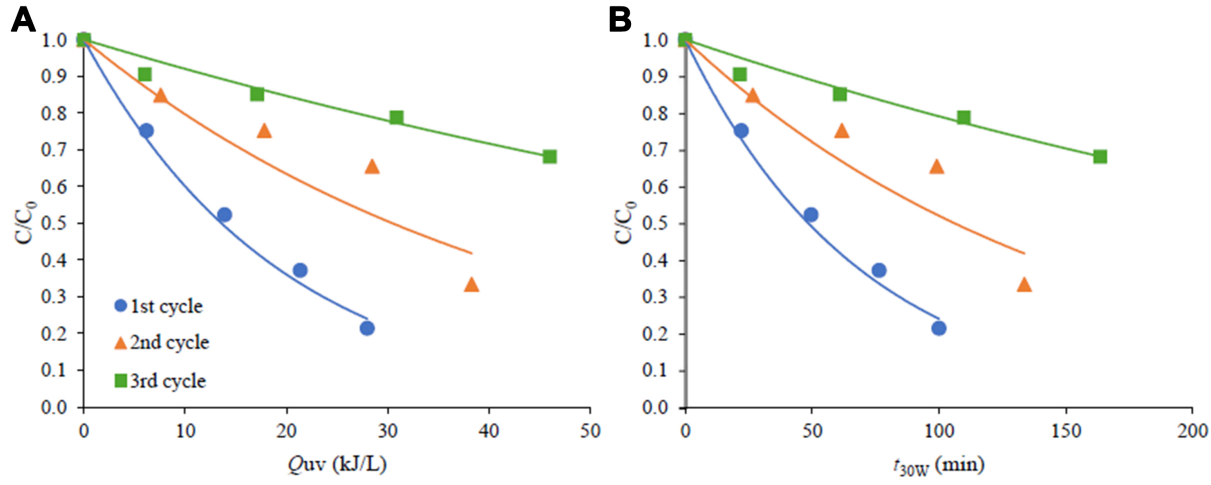

Figure 7. Degradation kinetics of PXT (C_0 = 20 μg/L) by reusing TiO_2 P-25 catalyst (300 mg/L) under natural solar irradiation as a function of Q_{UV} (A) and t_{30W} (B). PXT: Paroxetine.

higher catalyst concentrations (300 and 500 mg/L) are applied, the reaction rate decreases, and unwanted scattering of light and difficulty of its penetration into the solution may occur[33,51]. Of course, other factors such as pH, temperature, differences in the substrate's organic composition, *etc.*, affect the performance of heterogeneous photocatalysis[25,36,52-54], but it is believed that the intensity of radiation and the concentration of the catalyst effect are the most crucial factors in this case.

The reusability of the TiO_2 catalyst [Figure 7A and B] was also studied on a pilot scale for three consecutive days (three catalytic cycles), letting the photocatalyst settle down in the feed tank after the end of each experiment without washing it, and then used the next day (next catalytic cycle). Before the beginning of each experiment, WW was spiked with an appropriate volume of PXT solution, concluding at a concentration of 20 μg/L. The data obtained from this series of experiments are summarized in Table 4. In the first photocatalytic cycle, PXT is removed from WW at a rate of 78%. In the second cycle, it is removed

Table 4. Pseudo-first-order rate constant (k_{app}), correlation coefficient (R^2), % removal of PXT, and degree of degradation kinetic constant reduction (%Δk_{app}) for each catalytic cycle

TiO_2 P-25	PXT (20 μg/L)			
C = 300 mg/L	k_{app} (L/kJ)	R^2	%	Δk%
1st catalytic cycle	0.051	0.9932	78	-
2nd catalytic cycle	0.023	0.8876	66	54.9
3rd catalytic cycle	0.008	0.9276	32	65.2

PXT: Paroxetine.

by 66%, while in the third cycle, this percentage drops to 32%, indicating changes on the surface of the catalyst and, by extension, the decrease in its total active sites, resulting in deactivation. This phenomenon is also confirmed by the constant rate values of degradation (k_{app}) as they gradually decrease from cycle to cycle. Therefore, the separation of the catalyst from the suspension by an economical and efficient technique and, afterward, treatment to remove adsorbed substances should be studied in future studies. To evaluate the effectiveness of photocatalytic treatment in HWW amelioration, the physicochemical parameters Abs_{254}, total phenols, BOD_5, and COD were measured before and after substrate treatment [Table 5].

Results showed a reduction in Abs_{254} and total phenolic content after treatment, as shown in Table 5. The BOD_5/COD ratio was calculated to observe better the treated WW's quality, where a ratio of 1 indicates complete biodegradability. In contrast, the separate analysis of BOD_5 and COD alone does not fully explain the substrate's quality in the organic load. An increase in the BOD_5/COD ratio after each photocatalytic process was estimated in most cases, indicating enhanced biodegradability of the produced WW.

In vitro toxicity studies during the photocatalytic process (pilot-scale experiments)

Monitoring the toxicity of samples during photocatalytic processes is crucial for evaluating their effectiveness. The risk of increasing toxicity due to intermediate oxidation products makes it imperative to monitor toxicity levels during the application of AOPs[38,40]. The toxicity of the samples was evaluated by monitoring changes in the light intensity of the naturally luminescent bacterium *Vibrio fischeri*. The results obtained from samples collected at the beginning and end of each pilot-scale photocatalytic experiment are listed in Table 6. In general, the percentage of bioluminescence inhibition at the beginning of the photocatalytic treatment is generally low, except for the experiment with 200 mg/L of catalysts, where 65.81% bioluminescence inhibition was observed, indicating that this sample was highly toxic. In most cases, toxicity has been considerably decreased at the end of the process, while in some cases, the samples demonstrated the phenomenon of hormesis. Hormesis is the phenomenon in which the sample is not toxic enough to reduce the population of the *Vibrio fischeri* microorganism; instead, it contributes to its growth and, consequently, the intensity of the emitting light. In conclusion, significant or total detoxification of WW was demonstrated, and the elimination of PXT and its TPs and the amelioration of WW effluent quality with the decomposition of other organic compounds contributed to the initial toxicity observed in each experiment.

CONCLUSIONS

In lab-scale experiments, PXT concentration was degraded within a short time, up to 45 min, with slower removal of TOC and release of fluorine and nitrate anions. Thirteen TPs were identified, denoting hydroxylation, carbonylation, ether bond scission, fluorine atom substitution, and loss of CO_2 molecule degradation pathways of the parent compound and its derivatives.

Table 5. Abs_{254}, total phenols, BOD_5, COD values, and the BOD_5/COD ratio of HWW before and after treatment by TiO_2 in three consecutive PCC

TiO_2 (mg/L)	Abs_{254} (nm)			Total phenols (mg/L)			COD (mg/L)			BOD_5 (mg/L)			BOD_5/COD	
	0 min	300 min	% variation	0 min	300 min	% variation	0 min	300 min	% variation	0 min	300 min	% variation	0 min	300 min
200 mg/L	0.1596	0.1526	-4.39	1.241	1.102	-11.2	142	40	-71.8	47.9	23.6	-50.7	0.34	0.59
300 mg/L (1st PCC)	0.1793	0.1763	-1.67	1.079	0.948	-12.1	23	10	-56.5	2.1	5.6	166.7	0.09	0.56
300 mg/L (2nd PCC)	0.1699	0.1669	-1.77	1.468	1.281	-12.7	31	10	-67.7	8.7	1.7	-80.5	0.28	0.17
300 mg/L (3rd PCC)	0.1652	0.1597	-3.23	0.659	0.641	-2.61	47	20	-57.4	5.6	4.2	-25.0	0.12	0.21

BOD_5: Five-day biochemical oxygen demand; COD: chemical oxygen demand; HWW: hospital wastewater; PCC: photocatalytic cycles.

Assessing the *in silico* ecotoxicity of PXT and its TPs revealed, in most cases, less toxic TPs than the parent compound for the three species of aquatic organisms studied (fish, daphnid, and green algae). TP-328 and TP1-346 were identified as those TPs posing higher toxicity. Based on the TEST software predictions for mutagenicity, BCF, and developmental toxicity values, all TPs were classified as "developmental toxicant", with only TP-210 and TP-226 classified as mutagenic. The BCF values show that PXT is the only compound that tends to accumulate more in aquatic organisms.

In CPC pilot-scale photocatalytic experiments under environmentally relevant conditions, the most efficient PXT removal was achieved, with the catalyst's concentration being 200 mg/L. The reusability of the catalysts for three cycles indicated partial deactivation and the need for effective separation and regeneration to maintain catalytic efficiency. Pilot-scale photocatalytic treatment led to less or non-toxic (hormesis phenomenon) WW effluents.

In summary, TiO_2 P-25-photocatalysis effectively removes PXT and its TPs while ameliorating the physicochemical characteristics of effluents; however, more practical applications need to be explored, and future research should focus on efficient recovery and reactivation methods for photocatalysts. Additionally, reactor engineering, the synthesis of stable and efficient visible light catalysts, the influence of matrices on the catalysts' surface, and the estimation of toxicity in mixtures of contaminants or their metabolites are crucial for incorporating heterogeneous photocatalysis into WWTPs, particularly for eliminating PhACs.

The main purpose of employing heterogeneous photocatalysis as an alternative and more efficient method to conventional WW treatment lies in the degradation of toxic compounds, such as PhACs, that are not fully degraded in conventional WWTPs and can subsequently affect humans. Effectively managing WW in an economical and environmentally friendly manner is a significant challenge for society, which aims to eliminate sources of aquifer pollution while safeguarding human health.

Table 6. Toxicity study of pilot-scale photocatalytic experiments with different catalyst concentrations and catalyst reuse

Irradiation time (min)	% Bioluminescence inhibition of *Vibrio fischeri*					
	TiO_2 concentration			Cycles with TiO_2 (300 mg/L)		
	200 mg/L	300 mg/L	500 mg/L	1st cycle	2nd cycle	3rd cycle
0	65.81	17.90	21.11	13.59	20.74	15.73
300	30.85	Hormesis	3.75	6.72	Hormesis	4.89

DECLARATIONS

Acknowledgments

The authors would like to thank the Unit of Environmental, Organic, and Biochemical high-resolution analysis-ORBITRAP-LC–MS of the University of Ioannina for providing access to the facilities.

Authors' contributions

Investigation, formal analysis, visualization, writing - original draft and editing: Sioulas, S.
Investigation and formal analysis: Rapti, I.; Kosma, C.
Conceptualization, project administration, methodology, supervision, resources, writing - original draft preparation, and writing - review and editing: Konstantinou, I.
Conceptualization, project administration, methodology, supervision, resources: Albanis, T.

Availability of data and materials

The data presented in this study are available in this article and the associated Supplementary Materials.

Financial support and sponsorship

This research is co-financed by Greece and the European Union (European Social Fund- ESF) through the Operational Programme «Human Resources Development, Education and Lifelong Learning 2014-2020» in the context of the project "Chemistry and Technologies for Pollution Control and Environmental Protection (MIS 6004807)".

Conflicts of interest

Konstantinou, I. is the Guest Editor of the Special Issue "Recent Progress on Photocatalytic Treatment of Water and Wastewater" and an Editorial Board member of the journal *Water Emerging Contaminants & Nanoplastics*. Konstantinou, I. was no t involved in any steps of editorial processing, notably including reviewer selection, manuscript handling, and decision making. The other authors declared that there are no conflicts of interest.

Ethical approval and consent to participate

Not applicable.

Consent for publication

Not applicable.

REFERENCES

1. Ahmed, S.; Khan, F. S. A.; Mubarak, N. M.; et al. Emerging pollutants and their removal using visible-light responsive photocatalysis - a comprehensive review. *J. Environ. Chem. Eng.* **2021**, *9*, 106643. DOI
2. Lykos, C.; Kourkouta, T.; Konstantinou, I. Study on the photocatalytic degradation of metronidazole antibiotic in aqueous media with

TiO_2 under lab and pilot scale. *Sci. Total. Environ.* **2023**, *870*, 161877. DOI

3. Antonopoulou, M.; Kosma, C.; Albanis, T.; Konstantinou, I. An overview of homogeneous and heterogeneous photocatalysis applications for the removal of pharmaceutical compounds from real or synthetic hospital wastewaters under lab or pilot scale. *Sci. Total. Environ.* **2021**, *765*, 144163. DOI PubMed
4. Kaur, A.; Umar, A.; Kansal, S. K. Heterogeneous photocatalytic studies of analgesic and non-steroidal anti-inflammatory drugs. *Appl. Catal. A. Gen.* **2016**, *510*, 134-55. DOI
5. Kosma, C. I.; Kapsi, M. G.; Konstas, P. G.; et al. Assessment of multiclass pharmaceutical active compounds (PhACs) in hospital WWTP influent and effluent samples by UHPLC-Orbitrap MS: temporal variation, removals and environmental risk assessment. *Environ. Res.* **2020**, *191*, 110152. DOI PubMed PMC
6. Paíga, P.; Correia, M.; Fernandes, M. J.; et al. Assessment of 83 pharmaceuticals in WWTP influent and effluent samples by UHPLC-MS/MS: hourly variation. *Sci. Total. Environ.* **2019**, *648*, 582-600. DOI
7. Hernando, M. D.; Mezcua, M.; Fernández-Alba, A. R.; Barceló, D. Environmental risk assessment of pharmaceutical residues in wastewater effluents, surface waters and sediments. *Talanta* **2006**, *69*, 334-42. DOI PubMed
8. Gopinath, K. P.; Madhav, N. V.; Krishnan, A.; Malolan, R.; Rangarajan, G. Present applications of titanium dioxide for the photocatalytic removal of pollutants from water: a review. *J. Environ. Manage.* **2020**, *270*, 110906. DOI
9. Frédéric, O.; Yves, P. Pharmaceuticals in hospital wastewater: their ecotoxicity and contribution to the environmental hazard of the effluent. *Chemosphere* **2014**, *115*, 31-9. DOI
10. Hwang, S.; Kim, J. H.; Jo, S. H. Inhibitory effect of the selective serotonin reuptake inhibitor paroxetine on human Kv1.3 channels. *Eur. J. Pharmacol.* **2021**, *912*, 174567. DOI
11. Silva, L. J.; Pereira, A. M.; Meisel, L. M.; Lino, C. M.; Pena, A. A one-year follow-up analysis of antidepressants in Portuguese wastewaters: occurrence and fate, seasonal influence, and risk assessment. *Sci. Total. Environ.* **2014**, *490*, 279-87. DOI
12. Santoke, H.; Cooper, W. J. Environmental photochemical fate of selected pharmaceutical compounds in natural and reconstituted Suwannee River water: role of reactive species in indirect photolysis. *Sci. Total. Environ.* **2017**, *580*, 626-31. DOI PubMed
13. Gornik, T.; Carena, L.; Kosjek, T.; Vione, D. Phototransformation study of the antidepressant paroxetine in surface waters. *Sci. Total. Environ.* **2021**, *774*, 145380. DOI
14. Kwon, J. W.; Armbrust, K. L. Hydrolysis and photolysis of paroxetine, a selective serotonin reuptake inhibitor, in aqueous solutions. *Environ. Toxicol. Chem.* **2004**, *23*, 1394-9. DOI PubMed
15. Carvalho, P. S.; de, M. C. C.; Ayala, A. P.; Ellena, J. X-Ray diffraction, spectroscopy and thermochemical characterization of the pharmaceutical paroxetine nitrate salt. *J. Mol. Struct.* **2016**, *1118*, 288-92. DOI
16. Gurke, R.; Rößler, M.; Marx, C.; et al. Occurrence and removal of frequently prescribed pharmaceuticals and corresponding metabolites in wastewater of a sewage treatment plant. *Sci. Total. Environ.* **2015**, *532*, 762-70. DOI
17. Lajeunesse, A.; Smyth, S. A.; Barclay, K.; Sauvé, S.; Gagnon, C. Distribution of antidepressant residues in wastewater and biosolids following different treatment processes by municipal wastewater treatment plants in Canada. *Water. Res.* **2012**, *46*, 5600-12. DOI PubMed
18. Metcalfe, C. D.; Chu, S.; Judt, C.; et al. Antidepressants and their metabolites in municipal wastewater, and downstream exposure in an urban watershed. *Environ. Toxicol. Chem.* **2010**, *29*, 79-89. DOI
19. Schlüsener, M. P.; Hardenbicker, P.; Nilson, E.; Schulz, M.; Viergutz, C.; Ternes, T. A. Occurrence of venlafaxine, other antidepressants and selected metabolites in the Rhine catchment in the face of climate change. *Environ. Pollut.* **2015**, *196*, 247-56. DOI PubMed
20. Yuan, S.; Jiang, X.; Xia, X.; Zhang, H.; Zheng, S. Detection, occurrence and fate of 22 psychiatric pharmaceuticals in psychiatric hospital and municipal wastewater treatment plants in Beijing, China. *Chemosphere* **2013**, *90*, 2520-5. DOI
21. Duarte, P.; Almeida, C. M. R.; Fernandes, J. P.; et al. Bioremediation of bezafibrate and paroxetine by microorganisms from estuarine sediment and activated sludge of an associated wastewater treatment plant. *Sci. Total. Environ.* **2019**, *655*, 796-806. DOI
22. Ebele, A. J.; Abou-Elwafa, A. M.; Harrad, S. Pharmaceuticals and personal care products (PPCPs) in the freshwater aquatic environment. *Emerg. Contam.* **2017**, *3*, 1-16. DOI
23. Li, R.; Li, T.; Zhou, Q. Impact of titanium dioxide (TiO_2) modification on its application to pollution treatment - a review. *Catalysts* **2020**, *10*, 804. DOI
24. Oturan, M. A.; Aaron, J. Advanced oxidation processes in water/wastewater treatment: principles and applications. a review. *Crit. Rev. Env. Sci. Tec.* **2014**, *44*, 2577-641. DOI
25. Antoniou, M. G.; Zhao, C.; O'shea, K. E.; et al. CHAPTER 1. Photocatalytic degradation of organic contaminants in water: process optimization and degradation pathways. In: Dionysiou DD, Li Puma G, Ye J, Schneider J, Bahnemann D, editors. Photocatalysis. Cambridge: Royal Society of Chemistry; 2016. pp. 1-34. DOI
26. Fotiou, D.; Lykos, C.; Konstantinou, I. Photocatalytic removal of the antidepressant fluoxetine from aqueous media using TiO_2 P25 and g-C_3N_4 catalysts. *J. Environ. Chem. Eng.* **2024**, *12*, 111677. DOI
27. Vagi, M. C.; Petsas, A. S. Recent advances on the removal of priority organochlorine and organophosphorus biorecalcitrant pesticides defined by Directive 2013/39/EU from environmental matrices by using advanced oxidation processes: an overview (2007-2018). *J. Environ. Chem. Eng.* **2020**, *8*, 102940. DOI
28. Zhu, D.; Zhou, Q. Action and mechanism of semiconductor photocatalysis on degradation of organic pollutants in water treatment: a review. *Environ. Nanotechnol. Monit. Manag.* **2019**, *12*, 100255. DOI

29. Suleiman Khasawneh O, Palaniandy P. Removal of organic pollutants from water by Fe_2O_3/TiO_2 based photocatalytic degradation: a review. *Environ. Technol. Innov.* **2021**, *21*, 101230. DOI
30. Fujishima, A.; Rao, T. N.; Tryk, D. A. Titanium dioxide photocatalysis. *J. Photoch. Photobio. C.* **2000**, *1*, 1-21. DOI
31. Katal, R.; Masudy-Panah, S.; Tanhaei, M.; Farahani, M. H. D. A.; Jiangyong, H. A review on the synthesis of the various types of anatase TiO_2 facets and their applications for photocatalysis. *Chem. Eng. J.* **2020**, *384*, 123384. DOI
32. Velempini, T.; Prabakaran, E.; Pillay, K. Recent developments in the use of metal oxides for photocatalytic degradation of pharmaceutical pollutants in water - a review. *Mater. Today. Chem.* **2021**, *19*, 100380. DOI
33. Gaya, U. I.; Abdullah, A. H. Heterogeneous photocatalytic degradation of organic contaminants over titanium dioxide: a review of fundamentals, progress and problems. *J. Photoch. Photobio. C.* **2008**, *9*, 1-12. DOI
34. Mccullagh, C.; Skillen, N.; Adams, M.; Robertson, P. K. Photocatalytic reactors for environmental remediation: a review. *J. Chem. Tech. Biotech.* **2011**, *86*, 1002-17. DOI
35. Rapti, I.; Kosma, C.; Albanis, T.; Konstantinou, I. Solar photocatalytic degradation of inherent pharmaceutical residues in real hospital WWTP effluents using titanium dioxide on a CPC pilot scale reactor. *Catal. Today.* **2023**, *423*, 113884. DOI
36. Spasiano, D.; Marotta, R.; Malato, S.; Fernandez-Ibañez, P.; Di, S. I. Solar photocatalysis: materials, reactors, some commercial, and pre-industrialized applications. A comprehensive approach. *Appl. Catal. B. Environ.* **2015**, *170-1*, 90-123. DOI
37. Sundar, K. P.; Kanmani, S. Progression of photocatalytic reactors and it's comparison: a review. *Chem. Eng. Res. Des.* **2020**, *154*, 135-50. DOI
38. Brienza, M.; Mahdi, A. M.; Escande, A.; et al. Use of solar advanced oxidation processes for wastewater treatment: follow-up on degradation products, acute toxicity, genotoxicity and estrogenicity. *Chemosphere* **2016**, *148*, 473-80. DOI
39. Fernández-Ibáñez, P.; Blanco, J.; Malato, S.; de, N. F. J. Application of the colloidal stability of TiO_2 particles for recovery and reuse in solar photocatalysis. *Water. Res.* **2003**, *37*, 3180-8. DOI PubMed
40. Sousa, M.; Gonçalves, C.; Vilar, V. J.; Boaventura, R. A.; Alpendurada, M. Suspended TiO_2-assisted photocatalytic degradation of emerging contaminants in a municipal WWTP effluent using a solar pilot plant with CPCs. *Chem. Eng. J.* **2012**, *198-9*, 301-9. DOI
41. Konstas, P.; Kosma, C.; Konstantinou, I.; Albanis, T. Photocatalytic treatment of pharmaceuticals in real hospital wastewaters for effluent quality amelioration. *Water* **2019**, *11*, 2165. DOI
42. Babaeivelni, K.; Khodadoust, A. P. Adsorption of fluoride onto crystalline titanium dioxide: effect of pH, ionic strength, and co-existing ions. *J. Colloid. Interface. Sci.* **2013**, *394*, 419-27. DOI PubMed
43. Antonopoulou, M.; Dormousoglou, M.; Spyrou, A.; Dimitroulia, A. A.; Vlastos, D. An overall assessment of the effects of antidepressant paroxetine on aquatic organisms and human cells. *Sci. Total. Environ.* **2022**, *852*, 158393. DOI PubMed
44. Cunningham, V. L.; Constable, D. J.; Hannah, R. E. Environmental risk assessment of paroxetine. *Environ. Sci. Technol.* **2004**, *38*, 3351-9. DOI PubMed
45. Dmitriev, A.; Rudik, A.; Filimonov, D.; et al. Integral estimation of xenobiotics' toxicity with regard to their metabolism in human organism. *Pure. Appl. Chem.* **2017**, *89*, 1449-58. DOI
46. Diniz, R. R.; Domingos, T. F. S.; Pinto, G. R.; Cabral, L. M.; de, P. M.; de Souza, A. M. T. Use of in silico and in vitro methods as a potential new approach methodologies (NAMs) for (photo)mutagenicity and phototoxicity risk assessment of agrochemicals. *Sci. Total. Environ.* **2023**, *904*, 167320. DOI
47. Toropova, A. P.; Toropov, A. A.; Roncaglioni, A.; Benfenati, E. The enhancement scheme for the predictive ability of QSAR: a case of mutagenicity. *Toxicol. In. Vitro.* **2023**, *91*, 105629. DOI PubMed
48. Gómez-Regalado, M. D. C.; Martín, J.; Santos, J. L.; Aparicio, I.; Alonso, E.; Zafra-Gómez, A. Bioaccumulation/bioconcentration of pharmaceutical active compounds in aquatic organisms: assessment and factors database. *Sci. Total. Environ.* **2023**, *861*, 160638. DOI PubMed
49. Khan, K.; Kumar, V.; Colombo, E.; Lombardo, A.; Benfenati, E.; Roy, K. Intelligent consensus predictions of bioconcentration factor of pharmaceuticals using 2D and fragment-based descriptors. *Environ. Int.* **2022**, *170*, 107625. DOI PubMed
50. Sousa, M.; Gonçalves, C.; Pereira, J. H.; Vilar, V. J.; Boaventura, R. A.; Alpendurada, M. Photolytic and TiO_2-assisted photocatalytic oxidation of the anxiolytic drug lorazepam (Lorenin® pills) under artificial UV light and natural sunlight: a comparative and comprehensive study. *Sol. Energy.* **2013**, *87*, 219-28. DOI
51. Wetchakun, K.; Wetchakun, N.; Sakulsermsuk, S. An overview of solar/visible light-driven heterogeneous photocatalysis for water purification: TiO_2- and ZnO-based photocatalysts used in suspension photoreactors. *J. Ind. Eng. Chem.* **2019**, *71*, 19-49. DOI
52. Chen, D.; Cheng, Y.; Zhou, N.; et al. Photocatalytic degradation of organic pollutants using TiO_2-based photocatalysts: a review. *J. Clean. Prod.* **2020**, *268*, 121725. DOI
53. Chong, M. N.; Jin, B.; Chow, C. W.; Saint, C. Recent developments in photocatalytic water treatment technology: a review. *Water. Res.* **2010**, *44*, 2997-3027. DOI PubMed
54. Lin, L.; Jiang, W.; Chen, L.; Xu, P.; Wang, H. Treatment of produced water with photocatalysis: recent advances, affecting factors and future research prospects. *Catalysts* **2020**, *10*, 924. DOI